Available online at www.sciencedirect.com
SCIENCE DIRECT®
Comput. Methods Appl. Mech. Engrg. 193 (2004) 4417–4438
Computer methods in applied mechanics and engineering
www.elsevier.com/locate/cma

The material point method in large strain engineering problems

Z. Więckowski

Chair of Mechanics of Materials, Technical University of Łódź, Al. Politechniki 6, 90-924 Łódź, Poland

Received 3 April 2003; received in revised form 4 October 2003; accepted 12 January 2004

Abstract

The material point method is a variant of the finite element method formulated in an arbitrary Lagrangian–Eulerian description of motion. Two kinds of spatial discretization are utilized in the method—the motion of material points, representing subregions of the analysed continuum, is traced against a background of the computational element mesh. The mesh can be chosen arbitrarily so that the main disadvantage of the finite element method, related to mesh distortion, is avoided. Application of the method to some large strain industrial problems as granular flow in a silo as well as geomechanical and plastic forming problems are shown.

Keywords: Material point method; Finite element method; Arbitrary Lagrangian–Eulerian formulation; Large strains; Plasticity

1. Introduction

Some engineering problems as granular flow or plastic forming problems are still hard to analyse although many well-developed computational techniques are available. The finite element method (FEM), which is a computational tool used most frequently in engineering analyses, exhibits some disadvantages in the case of problems where very large strains occur. The main disadvantage of FEM—when formulated in the Lagrangian format—is related to the problem of mesh distortion. When the deformation process is developed, the original element mesh can suffer from high distortions so that the accuracy of the calculations is significantly deteriorated. The calculation process can even be impossible to continue when the Jacobian determinants become negative at some points of numerical integration. As a remedy, a mesh-rezoning technique can be employed in order to restore proper shapes of elements. The use of such a technique means that the fields of state variables have to be mapped from the distorted mesh to the newly generated one. This mapping is not a straight-forward task and introduces additional errors. On the other hand, the finite element method formulated in the Eulerian frame is not suitable in problems with free surfaces.

In order to avoid this disadvantage of the standard finite element method, other computational techniques have been investigated. One of them is the finite element method formulated in an arbitrary

E-mail address: zwi@p.lodz.pl (Z. Więckowski).

0045-7825/$ - see front matter
doi:10.1016/j.cma.2004.01.035

Lagrangian–Eulerian description of motion which—in conjunction with adaptive mesh techniques—enables to avoid the problem of mesh distortion. This approach has been investigated in many papers e.g. by Pracht [1], Hughes et al. [2], Belytschko et al. [3], Donea [4], van der Lugt and Huetink [5], Schreurs et al. [6], Liu et al. [7–9], Huerta and Liu [10] and Benson [11]. A detailed description of the arbitrary Lagrangian–Eulerian formulation of the finite element method is given in the book by Belytschko et al. [12] issued recently.

Another computational approach to the large strain problems is represented by the group of particle or point-based methods. These methods, called also meshless methods, overcome the main drawback of the finite element method related to mesh distortions. Their common feature is that the history of state variables is traced at points (particles) which are not connected with any element mesh the distortions of which is a source of numerical difficulties. With respect to an approximate technique used, the point-based methods can be classified in four basic groups: methods based on the moving weighted least square (MWLS) approximation, kernel methods, partition of unity methods, and the material point (particle-in-cell) method. Among the techniques based on the MWLS approximation, the following methods can be quoted: the meshless (generalised) finite difference method developed by Liszka and Orkisz [13] and Orkisz [14,15], the diffuse element method proposed by Nayroles et al. [16], the element-free Galerkin method by Belytschko et al. [17], the free particle method by Jach et al. [18], the finite point method by Oñate et al. [19], and the local meshless Petrov–Galerkin and boundary integral methods by Atluri and Zhu [20] and Zhu et al. [21]. The following methods belong to the group of kernel methods: the smoothed particle hydrodynamics (SPH) method investigated by Lucy [22], Monaghan [23], Libersky et al. [24], Johnson et al. [25], and Randles and Libersky [26], and the reproducing kernel particle method studied by Liu et al. [27], and Chen et al. [28]. Examples of the partition of unity method are: the partition of unity finite element method introduced by Melenk and Babuška [29], *h–p* clouds method by Duarte and Oden [30], and the method elaborated by Liszka et al. [31] which links the concepts of the MWLS and finite difference methods. The description of the point-based methods is given in the books by Zienkiewicz and Taylor [32] and Liu [33].

Among the above-mentioned methods, the material point method (MPM), introduced originally in fluid dynamics by Harlow (see [34] and references therein) and known as the particle-in-cell (PIC) method, has been applied successfully to the problems of solid mechanics by Burgess et al. [35] and Sulsky et al. [36–38]. The material point method can be regarded as the finite element method formulated in an arbitrary Lagrangian–Eulerian description of motion. It can also be classified as a meshless method. In the material point method, state variables for the analysed body are traced at the set of points (material points) defined independently of an Eulerian mesh (computational mesh) on which the equations of motion are formulated and solved. As the computational mesh can be defined in an arbitrary way, the problem of mesh distortion, which leads to difficulties in an Lagrangian formulation of FEM, is avoided.

On the basis of the knowledge presented in above-mentioned papers [35–38], the use of the material point method has been extended on the frictional contact problem by Więckowski et al. [39]. Unlike in the papers [35–38], where regular rectangular element mesh has been used, the triangular elements have been employed in [39] which enables to analyse bodies of arbitrary geometry.

In the present paper, an improvement of the material point procedure is proposed—the field of the mass density of the material is calculated using the current position of the material points in contrast to the approach shown in [39] where the formula for the change of the determinant of the local Jacobian matrix (calculated for the material points) has been exploited. The new procedure of determining the mass density field extends the range of problems possible to analyse. It enables to solve the problems where the mass density is involved in the constitutive relations, e.g. in the case when the first invariant of the stress tensor depends on the mass density. The procedure gives smooth field of pressure which leads to higher accuracy of the computational results. Moreover, new applications of the material point method are shown in the paper. The problem of silo flow of the granular material around an insert is analysed. This problem is very

difficult to solve when the purely Lagrangian formulation of the finite element method is used. The other problems analysed in the paper are: silo filling, land slide and plastic forming. Two-dimensional problems are under investigation: the plane strain problem and the axisymmetric one.

2. Material point method—description

Let $\Omega \subset \mathbb{R}^3$ denote the region occupied by an analysed body at time $t \in I \equiv [0, T]$ $(T > 0)$. Let $\partial\Omega$ denote the boundary of region Ω, which consists of three parts Γ_u, Γ_σ where displacements and stresses are given, respectively, and Γ_c where the frictional contact problem is to be solved. Let ϱ denote the mass density, a_i and w_i the vectors of acceleration and weighting functions, respectively, σ_{ij} and t_i the Cauchy stress tensor and vector, respectively, b_i the vector of volumetric forces, and n_i the unit vector outwardly normal to $\partial\Omega$. As in the standard finite element method, the equation of virtual work is used as the starting point in the formulation of the material point method

$$\int_\Omega \varrho\left(a_i w_i + \frac{1}{\varrho}\sigma_{ij} w_{i,j}\right) \mathrm{d}x = \int_\Omega \varrho b_i w_i \,\mathrm{d}x + \int_{\Gamma_\sigma} t_i w_i \,\mathrm{d}s + \int_{\Gamma_c} \sigma_{ij} n_j w_i \,\mathrm{d}s \quad \forall \boldsymbol{w} \in V_0, \tag{1}$$

where $V_0 = \{\boldsymbol{w} : \ w_i = 0 \text{ on } \Gamma_u\}$ denotes the space of displacement fields satisfying the homogeneous boundary conditions which are sufficiently regular in the sense of all mathematical operations required. In order to complete the dynamic problem, the initial conditions are considered in the following form:

$$u_i(0) = u_i^0, \quad \dot{u}_i(0) = v_i^0, \quad \sigma_{ij}(0) = \sigma_{ij}^0,$$

where u_i^0, v_i^0 and σ_{ij}^0 denotes the initial fields of displacements, velocities and stresses, respectively.

Two kinds of space discretization are used in the material point method. Firstly, the initial configuration of the analysed body is divided into a finite number of subregions. Each of these subregions is represented by one of its points, called a material point. It is assumed that the whole mass of the specific subregion is concentrated at the corresponding material point, so that the mass density field can be expressed as follows:

$$\varrho(\boldsymbol{x}) = \sum_{P=1}^{N} M_P \delta(\boldsymbol{x} - \boldsymbol{X}_P), \tag{2}$$

where M_P and $\boldsymbol{X}_P$ are mass and position of the Pth material point, respectively, $\delta(\boldsymbol{x})$ denotes the Dirac delta function, and N is the number of material points. On the other hand, the equation of virtual work is formulated and solved in the Eulerian frame by the use of a computational mesh. This mesh can be chosen arbitrarily, which implies that the problem of mesh distortion does not appear in this formulation. Both the kinds of space discretization are illustrated in Fig. 1.

Using Eq. (2), we can write the equation of virtual work in the following form:

$$\sum_{P=1}^{N} M_P\left[a_i(\boldsymbol{X}_P) w_i(\boldsymbol{X}_P) + \sigma_{ij}^{\varrho}(\boldsymbol{X}_P) w_{i,j}(\boldsymbol{X}_P)\right] = \sum_{P=1}^{N} M_P b_i(\boldsymbol{X}_P) w_i(\boldsymbol{X}_P) + \int_{\Gamma_\sigma} t_i w_i \,\mathrm{d}s + \int_{\Gamma_c} \sigma_{ij} n_j w_i \,\mathrm{d}s, \tag{3}$$

where $\sigma_{ij}^{\varrho} = \sigma_{ij}/\varrho$. The same equation is obtained in the case of the axisymmetric problem as the field of mass density can be represented as

$$\varrho(\boldsymbol{x}) = \sum_{P=1}^{N} \frac{M_P}{2\pi x} \delta(\boldsymbol{x} - \boldsymbol{X}_P), \tag{4}$$

where variables (x, y, Θ) are used instead of (r, z, Θ).

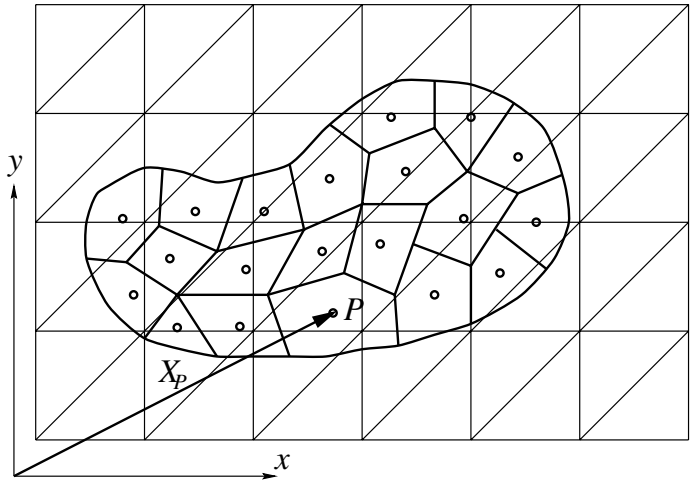

Fig. 1. Space discretization—material points and computational mesh.

Let fields a_i and w_i be approximated as follows (the two-dimensional case is considered):

$$\boldsymbol{a}(\boldsymbol{x},t) \equiv \left\{ \begin{array}{c} a_x \\ a_y \end{array} \right\} = \mathbf{N}\mathbf{a}, \quad \boldsymbol{w}(\boldsymbol{x},t) \equiv \left\{ \begin{array}{c} w_x \\ w_y \end{array} \right\} = \mathbf{N}\mathbf{w}, \tag{5}$$

where $\mathbf{N}$ is the matrix of global shape functions defined for the whole computational mesh,

$$\mathbf{N}(\boldsymbol{x}) = \left[\begin{array}{cccccccc} N_1(\boldsymbol{x}) & 0 & N_2(\boldsymbol{x}) & 0 & \cdots & N_n(\boldsymbol{x}) & 0 \\ 0 & N_1(\boldsymbol{x}) & 0 & N_2(\boldsymbol{x}) & \cdots & 0 & N_n(\boldsymbol{x}) \end{array} \right],$$

$$\mathbf{a} = [\, a_{1x} \quad a_{1y} \quad a_{2x} \quad \cdots \quad a_{nx} \quad a_{ny} \,]^{\mathrm{T}}$$

and

$$\mathbf{w} = [\, w_{1x} \quad w_{1y} \quad w_{2x} \quad \cdots \quad w_{nx} \quad w_{ny} \,]^{\mathrm{T}}$$

are nodal values of fields a_i and w_i, respectively, n denotes the number of nodes in the computational grid.

Let us define the following vectors for the case of two-dimensional problems:

$$\boldsymbol{s}^{\varrho} = \frac{1}{\varrho} \left\{ \begin{array}{c} \sigma_{xx} \\ \sigma_{yy} \\ \sigma_{xy} \\ \hline \sigma_{\Theta\Theta} \end{array} \right\}, \quad \mathrm{b} = \left\{ \begin{array}{c} b_x \\ b_y \end{array} \right\}, \quad \mathrm{t} = \left\{ \begin{array}{c} t_x \\ t_y \end{array} \right\},$$

where the last term of vector $\boldsymbol{s}^{\varrho}$ appears only in the case of the axisymmetric problem. Using relations (5) in Eq. (3), we can write the problem in the discretized form as follows:

$$\mathbf{w}^{\mathrm{T}} \sum_{P=1}^{N} M_P \mathbf{N}^{\mathrm{T}}(\boldsymbol{X}_P)\mathbf{N}(\boldsymbol{X}_P)\mathbf{a} + \mathbf{w}^{\mathrm{T}} \sum_{P=1}^{N} M_P \mathbf{B}^{\mathrm{T}}(\boldsymbol{X}_P)\boldsymbol{s}^{\varrho}(\boldsymbol{X}_P) = \mathbf{w}^{\mathrm{T}} \sum_{P=1}^{N} M_P \mathbf{N}^{\mathrm{T}}(\boldsymbol{X}_P)\mathbf{b}(\boldsymbol{X}_P) + \mathbf{w}^{\mathrm{T}} \int_{\Gamma_\sigma} \mathbf{N}^{\mathrm{T}}\mathbf{t}\,\mathrm{d}s + \mathbf{w}^{\mathrm{T}}\mathbf{F}_c.$$

As vector $\mathbf{w}$ is arbitrary except the degrees of freedom defined at the nodes belonging to Γ_u, we obtain the following system of equations:

$$\mathbf{Ma} = \mathbf{F} + \mathbf{F}_c - \mathbf{R}. \tag{6}$$

The notation used in the two last equations is as follows:

$$\mathbf{M} = \sum_{P=1}^{N} M_P \mathbf{N}^{\mathrm{T}}(\boldsymbol{X}_P)\mathbf{N}(\boldsymbol{X}_P)$$

is the mass matrix depending on the position of the material points with respect to the computational mesh,

$$\mathbf{F} = \sum_{P=1}^{N} M_P \mathbf{N}^{\mathrm{T}}(\boldsymbol{X}_P)\mathbf{b}(\boldsymbol{X}_P) + \int_{\Gamma_\sigma} \mathbf{N}^{\mathrm{T}}\mathbf{t}\,\mathrm{d}s \tag{7}$$

is the vector of nodal external forces,

$$\mathbf{R} = \sum_{P=1}^{N} M_P \mathbf{B}^{\mathrm{T}}(\boldsymbol{X}_P)\boldsymbol{s}^{\varrho}(\boldsymbol{X}_P)$$

is the vector of nodal internal forces, and the definition of contact forces follows from the relation

$$\mathbf{w}^{\mathrm{T}}\mathbf{F}_c = \int_{\Gamma_c} \sigma_{ij} n_j w_i \,\mathrm{d}s.$$

Matrix $\mathbf{B}$ has the same structure as the strain–displacement matrix used in the standard finite element method

$$\mathrm{B}(\boldsymbol{X}_P) = \left[\begin{array}{cccc|c} \dfrac{\partial N_1(\boldsymbol{X}_P)}{\partial x} & 0 & \dfrac{\partial N_2(\boldsymbol{X}_P)}{\partial x} & 0 & \cdots \\ 0 & \dfrac{\partial N_1(\boldsymbol{X}_P)}{\partial y} & 0 & \dfrac{\partial N_2(\boldsymbol{X}_P)}{\partial y} & \cdots \\ \dfrac{\partial N_1(\boldsymbol{X}_P)}{\partial y} & \dfrac{\partial N_1(\boldsymbol{X}_P)}{\partial x} & \dfrac{\partial N_2(\boldsymbol{X}_P)}{\partial y} & \dfrac{\partial N_2(\boldsymbol{X}_P)}{\partial x} & \cdots \\ \hline \dfrac{N_1(\boldsymbol{X}_P)}{x} & 0 & \dfrac{N_2(\boldsymbol{X}_P)}{x} & 0 & \cdots \end{array}\right],$$

where the last row exists in the case of axisymmetric problems.

Because of the Dirac delta function representation of the mass density (2), the mass matrix is singular when its consistent form is considered. To solve system (6), the diagonalized matrix, $\mathbf{M}_l$, or nearly consistent matrix, $\mathbf{M}_\alpha = \alpha\mathbf{M} + (1-\alpha)\mathbf{M}_l$, can be used instead of $\mathbf{M}$, where $0 \leqslant \alpha < 1$ [35]. This idea follows the concept of "higher-order mass" (e.g. [40]). The diagonalized matrix, calculated by summing all terms in rows, is employed in this paper.

3. Incremental solution to the dynamic equations

The solution to the dynamic system (6) is found for a discrete set of instants $t_1, t_2, \ldots, t, t+\Delta t, \ldots \in I$ ($I \equiv [0, T]$, $0 < t_1 < t_2 < \cdots < t < t+\Delta t \cdots < T$). Using the explicit time integration procedure, the vector of nodal accelerations, $\mathbf{a}^{t+\Delta t}$, is calculated by solving the system of equations (6)

$$\mathbf{M}^t\mathbf{a}^{t+\Delta t} = \mathbf{F}^t + \mathbf{F}_c^t - \mathbf{R}^t$$

and the vector of nodal velocities, $\mathbf{v}^{t+\Delta t}$, from the relation

$$\mathbf{v}^{t+\Delta t} = \mathbf{v}^{t} + \Delta t \mathbf{a}^{t+\Delta t}.$$

Each time increment consists of two steps: the Lagrangian step and the convective one.

In the Lagrangian step, the calculations are performed in a similar way as in the updated Lagrangian formulation of the standard finite element method—it is assumed that the computational mesh deforms together with the considered body. The kinematic state variables are calculated for each material point by the use of interpolation functions and nodal parameters defined on the computational mesh. Particularly, the velocity vector for the Pth material point, $\mathbf{V}_P \equiv [\, V_{Px} \quad V_{Py} \,]^{\mathrm{T}}$, is calculated from the formula

$$\mathbf{V}_P = \mathbf{N}(\boldsymbol{X}_P)\mathbf{v}^{\mathrm{e}}, \tag{8}$$

where

$$\mathbf{v}^{\mathrm{e}} = [\, v_{1x} \quad v_{1y} \quad v_{2x} \quad v_{2y} \quad \cdots \quad v_{n_{\mathrm{e}}x} \quad v_{n_{\mathrm{e}}y} \,]^{\mathrm{T}}$$

is the vector of the nodal velocities of the element inside which the material point is located. Then the vector of the strain increment is calculated by the use of the matrix $\mathbf{B}$ as follows:

$$\Delta\mathbf{e} = \Delta t \mathbf{B}(\boldsymbol{X}_P)\mathbf{v}^{\mathrm{e}},$$

where $\Delta\mathbf{e} = \Delta t[\, d_{xx} \quad d_{yy} \quad d_{xy} \,]^{\mathrm{T}}$ or $\Delta\mathbf{e} = \Delta t[\, d_{xx} \quad d_{yy} \quad d_{xy} \quad d_{\Theta\Theta} \,]^{\mathrm{T}}$ for the plane strain and axisymmetric problems, respectively. Having calculated the strain increment, stresses can be obtained for each material point by integration of the constitutive relations.

The convective step consists in mapping the velocity field from the material points to the computational mesh. The mesh can be changed freely or remain in the same position as defined at the beginning of the time increment. Nodal velocities

$$\mathbf{v} = [\, v_{1x} \quad v_{1y} \quad v_{2x} \quad v_{2y} \quad \cdots \quad v_{nx} \quad v_{ny} \,]^{\mathrm{T}},$$

where n denotes the number of nodes in the computational mesh, are calculated by solving the following least square problem:

$$\sum_{P=1}^{N} M_P[\mathbf{N}(\mathbf{X}_P)\mathbf{v} - \mathbf{V}_P]^{\mathrm{T}}[\mathbf{N}(\mathbf{X}_P)\mathbf{v} - \mathbf{V}_P] = \min,$$

where masses of the material points play roles of weights. The vector of nodal velocities minimizing the above function is the solution to the following set of equations [35–38]

$$\mathbf{M}\mathbf{v} = \mathbf{S}^{\mathrm{T}}\mathbf{M}_d\mathbf{V}, \tag{9}$$

which expresses equivalence of momentum calculated for the material points and for the computational grid, where

$$\mathbf{V} = [\, V_{1x} \quad V_{1y} \quad V_{2x} \quad V_{2y} \quad \cdots \quad V_{Nx} \quad V_{Ny} \,]^{\mathrm{T}}$$

is the vector of velocities of all the material points, and matrices $\mathbf{S}$ and $\mathbf{M}_d$ are defined as follows:

$$\mathbf{S} = \begin{bmatrix} \mathbf{N}(\boldsymbol{X}_1) \\ \mathbf{N}(\boldsymbol{X}_2) \\ \vdots \\ \mathbf{N}(\boldsymbol{X}_N) \end{bmatrix}, \quad \mathbf{M}_d = \begin{bmatrix} \mathbf{M}_1 & \mathbf{0} & \cdots & \mathbf{0} \\ \mathbf{0} & \mathbf{M}_2 & \cdots & \mathbf{0} \\ \vdots & \vdots & \ddots & \vdots \\ \mathbf{0} & \mathbf{0} & \cdots & \mathbf{M}_N \end{bmatrix}, \quad \mathbf{M}_i = \begin{bmatrix} M_i & 0 \\ 0 & M_i \end{bmatrix}.$$

3.1. Time integration of the constitutive relations

The elastic–viscoplastic plastic and elastic–perfectly plastic constitutive models have been applied in the paper to describe the mechanical behaviour of the material in the analysed problems. The constitutive relations are integrated in time by the use of the backward Euler algorithm (e.g. [41]).

3.2. Solution to the frictional contact problem

The problem of unilateral contact of the part of the surface of the analysed body, Γ_c, with rigid obstacle having fixed position in time is solved. The phenomenon of friction is taken into consideration; the simplest case of the friction condition is implemented—the Coulomb friction condition

$$f_c(\sigma_N, \boldsymbol{\sigma}_T) = -\mu|\sigma_N| + \|\boldsymbol{\sigma}_T\| \leqslant 0, \tag{10}$$

where σ_N and $\boldsymbol{\sigma}_T$ denote the normal and tangential components of the Cauchy stress vector, respectively, μ is the friction coefficient, and $\|\cdot\|$ denotes the Euclidean norm of a vector.

The variational formulation of the contact problem for deformable bodies leads to the implicit variational inequality, some terms of which are non-differentiable functionals, which makes the problem difficult to solve. To overcome these troubles, the penalty regularization method is used for the law of frictional contact. The frictional contact problem is solved by calculation of the contact forces at the nodes of the computational mesh. Such an approach does not require introducing elements of node–segment type and is relatively easy to implement when the computational mesh is constant in time for the entire analysis. All the details related to the regularized contact law and procedure of calculation of nodal contact forces have been shown in [39].

3.3. Calculation of the density field

The field of mass density is calculated for each time increment at any material point from the formula

$$\varrho^{t+\Delta t} = (J_t^{t+\Delta t})^{-1}\varrho^t, \tag{11}$$

where ϱ^t and $\varrho^{t+\Delta t}$ are the density values calculated for instants t and $t+\Delta t$, respectively, and $J_t^{t+\Delta t}$ denotes the Jacobian determinant of the deformation gradient calculated for time $t+\Delta t$ and related to the configuration at time t. In the present paper, the above formula has been used in the analyses of such problems, where the mass density is not involved in constitutive relations.

Numerical calculations show that Eq. (11) can lead to significant numerical inaccuracies in some problems, for example, in a contact–impact problem for a material with pressure–volume change dependency. Especially, in the case of granular flow when stresses are equal to zero at the beginning of the process (e.g. in the case of process of filling a silo), calculation of volume change for the granular material—and the mass density and pressure in the sequel—is not sufficiently accurate if the density value is determined by the use of the local rule (11) for the material points. For this case, in the present paper, the mass density field of the flowing material is evaluated by the use of the current position of the material points. The field is approximated according to the following formula:

$$\varrho(\boldsymbol{x}) = \sum N_i\varrho_i, \tag{12}$$

where N_i is a shape function of an element of the computational mesh, ϱ_i a nodal value of mass density which—in the case of triangular elements with linear shape functions—is calculated as follows:

$$\varrho_i = \frac{\sum_{j=1}^{n_P}\sum_{P=1}^{P_j} N_i(\boldsymbol{X}_P)M_P}{\sum_{j=1}^{n_P} A_j/3}, \tag{13}$$

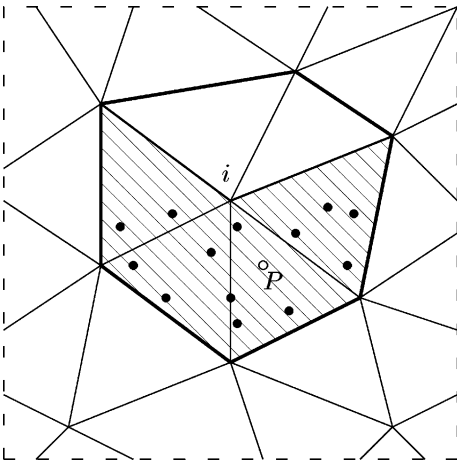

Fig. 2. Calculation of mass density field.

where P_j denotes the number of material points localised in the jth element, n_P the number of elements surrounding the ith node and including at list one material point (the hatched part of the patch shown in Fig. 2), A_j the area or the volume of the jth element in the plane strain or axisymmetric case, respectively. The shape functions, N_i, play the role of weights in Eq. (13).

3.4. Stability

It was shown in Ref. [39] that the explicit procedure of time integration of the dynamic equations required the shorter time increment when the material point method is utilized than in the case of using the finite element method. The critical value of the time step depends on the current position of the material points with respect to the position of the elements of the computational mesh. It follows from the stability analysis given in [39] that increasing the number of material points increases the critical value of the time step.

3.5. Overall procedure

The overall procedure solving the dynamic problem by the material point method may be described as below.

1. Initialize the state variables for the material points and the time value, $t := 0$.
2. Beginning of calculation for one time step. Calculate velocities at mesh nodes, $\mathbf{v}^t$, solving the system of equations (9)

$$\mathbf{M}^t\mathbf{v}^t = (\mathbf{S}^t)^{\mathrm{T}}\mathbf{M}_d\mathbf{V}^t.$$

3. Calculate the vector of nodal internal forces, $\mathbf{R}^t$,

$$\mathbf{R}^t = \sum_{P=1}^{N} M_P\mathbf{B}^{\mathrm{T}}(\boldsymbol{X}_P^t)\boldsymbol{s}^t.$$

4. Calculate the vector of nodal forces, $\mathbf{F}^t$, equivalent to gravitational forces, according to Eq. (7), and frictional forces, $\mathbf{F}_c^t$, according to Section 3.2.

5. Calculate the vector of nodal accelerations by solving the system of equations

$$\mathbf{M}^t\mathbf{a}^{t+\Delta t} = \mathbf{F}^t + \mathbf{F}_c^t - \mathbf{R}^t.$$

6. Calculate the velocities of the material points

$$\mathbf{V}_P^{t+\Delta t} = \mathbf{V}_P^t + \Delta t\mathbf{N}(\mathbf{X}_P^t)\mathbf{a}^{t+\Delta t}, \quad P = 1, \ldots, N.$$

7. Calculate the nodal velocities, $\mathbf{v}^L$, related to updated velocities of the material points, by solving the system of equations

$$\mathbf{M}^t\mathbf{v}^L = (\mathbf{S}^t)^{\mathrm{T}}\mathbf{M}_d\mathbf{V}^{t+\Delta t}. \tag{14}$$

8. Calculate strain increment and spin at each material point using vector $\mathbf{v}^L$. Update stresses $\boldsymbol{s}^{t+\Delta t}$ and mass density as described in Section 3.3.
9. Update position of the material points

$$\boldsymbol{X}_P^{t+\Delta t} = \boldsymbol{X}_P^t + \Delta t\mathbf{N}(\boldsymbol{X}_P^t)\mathbf{v}^L, \quad P = 1, \ldots, N.$$

10. Set $t := t + \Delta t$. Exit procedure if $t > T$ or go to point 2 otherwise.

In the above procedure, the nodal vector $\mathbf{v}^L$ is used in order to calculate stresses instead of $\mathbf{v}^t + \Delta t\mathbf{a}^{t+\Delta t}$. If the latter was used, some material points, located near the free boundary would separate from the rest of the body. This is possible when the position of an only material point in an element approaches the element boundary, which implies that some terms of the element mass matrix tend to zero while the corresponding terms of the vector of nodal internal forces do not. The use of vector $\mathbf{v}^L$ for obtaining stresses smooths the field of accelerations—this procedure has been proposed by Sulsky et al. [37].

4. Advantages and disadvantages of the material point method

As other arbitrary Lagrangian–Eulerian approaches, the material point method links advantages of both the purely Lagrangian and purely Eulerian formulations of the finite element method and eliminates their drawbacks. The advantages are manifested in several aspects:

- The problem of mesh distortion characteristic of Lagrangian FEM is eliminated.
- The problem of free surface is easy to solve.
- The problem of flow around an obstacle is easy to solve as in the case of the Eulerian formulation.
- The problem of self-contact is solved automatically in the case of granular material—there is no penetration of particles because the velocities of the material point are calculated by interpolation of nodal values defined on the Eulerian mesh (see Eq. (8)).
- The boundary conditions can be applied as easily as in the case of standard FEM.
- External forces can be applied at nodes of the computational mesh or—if more suitable—at the material points.
- Adding material points during calculations is relatively easy. This is needed, for example, in the analysis of filling a silo.
- The material point method can be implemented in the standard finite element computer program in a relatively easy way.

The main drawback of the material point method is related to the condition of stability for the procedure of time integration of dynamic equations. The critical value for the time increment can be significantly

smaller than in the case of standard FEM. However, as mentioned in Section 3.4, the problem can be eased by increasing the number of material points.

Another disadvantage of the material method is that it is time consuming. However, it should be noted that the analysis of transient dynamic problems usually need rather long computation time. This drawback can be smoothed by implementation of parallel computation techniques. These techniques can be easily applied to the calculations performed on the elements and material points level, and also in solving the global system of equations when the diagonalisation of its matrix is used.

5. Numerical examples

5.1. Application to problems of granular flow in a silo

The problems of flow of a granular material during a process of discharging and filling a silo is interesting not only from the view-point of a designer that should determine interactions between the flowing material and silo walls but also from the view-point of a user that should predict the flow pattern and the flow rate for the stored material.

Due to the fact that the problem is of high complexity, various kinds of simplifications have been used in the analysis of such processes to estimate wall tractions and determine the flow pattern for the flowing material. Starting from 80s of the previous century, some researchers have applied various numerical approaches in order to solve this problem formulated properly from the view-point of continuum mechanics. Eibl and coworkers solved the problem of silo discharge using the finite element method [42,43]. They used an Eulerian description of motion in their analysis and treated the flowing granular material as a fluid. Such an approach is very useful when the region occupied by the flowing material is constant in time which means that the silo is refilled continuously with the material. This approach was used also by other researchers [44,45]. On the other hand, the use of the finite element method formulated in the Lagrangian description of motion is useful when the entire process of silo discharge is analysed. This approach accompanied with mesh-rezoning, applied in order to restore proper shapes of elements which are subjected to large distortions, has been presented in [46]. The entire process of silo discharge as well as the filling process can be solved by the discrete element method [47–49] in which the granular material is treated as a set of balls or cylinders usually of equal diameter. It seems, however, that this method is limited to the case when the ratio between the diameter of a silo outlet and the diameter of a grain is not very large. In order to eliminate disadvantages of the Lagrangian approach to the finite element method, related to large elements' distortions, the material point method has been utilized to the silo discharge problem by the author of the present paper and his co-workers [39], and recently by Oger et al. [50] and Mühlhaus et al. [49].

5.1.1. Granular flow in silo—discharge problem

Two examples of axisymmetric flow are considered for silos with flat bottoms, the cross-sections of which are shown in Fig. 3. The dimensions shown in the figure are given in centimetres. The silo, the cross-section of which is depicted on the right side of the figure, is equipped with inserts controlling the flow.

In the analysis of the problem, the constitutive behaviour of the granular material is described by the elastic–viscoplastic model with the Drucker–Prager yield condition and non-associated flow rule. Let s_{ij} and e_{ij} denote the deviatoric parts of the stress and rate-of-deformation tensors, σ_{ij} and d_{ij}, respectively,

$$s_{ij} = \sigma_{ij} + p\delta_{ij}, \quad \text{where } p = -\tfrac{1}{3}\sigma_{ii},$$

$$e_{ij} = d_{ij} - \tfrac{1}{3}d_{kk}\delta_{ij}$$

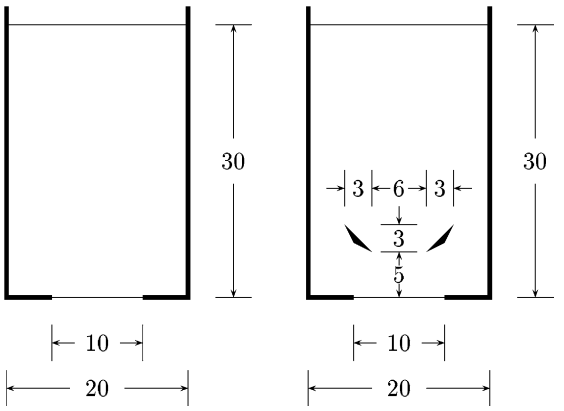

Fig. 3. Cross-sections of analysed silos—axisymmetric flow.

and p and q are invariants of the stress tensor

$$p = -\frac{1}{3}\sigma_{ii}, \quad q = \sqrt{\frac{3}{2}s_{ij}s_{ij}}.$$

Let B denote the set of plastically admissible stresses

$$B = \{\tau_{ij} : f(\tau_{ij}) \equiv q - mp \leqslant 0\},$$

where parameter m depends on the angle of internal friction, φ,

$$m = 18\sin\varphi/(9 - \sin^2\varphi).$$

The applied constitutive relations can be written in the form:

$$\dot{p} = Kd_{kk}, \tag{15}$$

$$e_{ij} = e^{\mathrm{e}}_{ij} + e^{\mathrm{vp}}_{ij}, \tag{16}$$

$$e^{\mathrm{e}}_{ij} = \frac{1}{2G}\overset{\nabla}{s}_{ij}, \tag{17}$$

$$e^{\mathrm{vp}}_{ij} = \gamma\langle\Phi(f)\rangle\frac{\partial g}{\partial\sigma_{ij}}, \tag{18}$$

where $\overset{\nabla}{s}_{ij}$ is the Jaumann–Zaremba measure of the stress-rate tensor, K and G are the bulk and shear moduli, respectively, expressed by Young modulus E and Poisson ratio v as follows: $K = E/(3(1-2v))$, $G = E/(2(1+v))$. Symbol γ in Eq. (18) denotes the viscosity parameter, while the function defining the viscoplastic flow has the form (e.g. [51]):

$$\Phi(f(\sigma_{ij})) = \left(\frac{q - mp}{mp}\right)^N, \quad N > 0,$$

where the meaning of parentheses $\langle\ \rangle$ is as follows:

$$\langle\Phi(f)\rangle = \begin{cases} \Phi(f) & \text{if } f > 0, \\ 0 & \text{if } f \leqslant 0. \end{cases}$$

The above constitutive relations are viscoplastic regularization of the elastic–perfectly plastic relations applied in the analysis of the silo discharge problem in Ref. [39,44,46].

As mentioned in Section 3.1, the time integration of the constitutive relations is performed according to the backward Euler rule, e.g. [41]. It can be shown—after some derivation—that the stress deviator corresponding to time $t + \Delta t$ may be expressed by the formula

$$s_{ij}^{t+\Delta t} = \frac{s_{ij}^{\mathrm{e}}}{1 + \dfrac{3G}{q}\Delta\bar{e}^{\mathrm{vp}}}, \tag{19}$$

where s_{ij}^{e} is the deviatoric part of trial "elastic" stresses

$$s_{ij}^{\mathrm{e}} = s_{ij}^{t} + 2G\Delta e_{ij}, \tag{20}$$

q is the invariant of stresses $s_{ij}^{t+\Delta t}$ calculated as follows:

$$q = q^{\mathrm{e}} - 3G\Delta\bar{e}^{\mathrm{vp}}, \tag{21}$$

where $\Delta\bar{e}^{\mathrm{vp}}$, the plastic strain factor, is the solution of the following non-linear equation

$$\Delta\bar{e}^{\mathrm{vp}} = \gamma\Delta t\left(\frac{q^{\mathrm{e}} - mp - 3G\Delta\bar{e}^{\mathrm{vp}}}{mp}\right)^{N}. \tag{22}$$

In Eqs. (20) and (21), s_{ij}^{t} denotes the deviatoric stresses calculated for the previous time increment, t, Δe_{ij} the deviatoric part of the strain increment, and q^{e} the invariant of the trial stress tensor, s_{ij}^{e}. When $N = 1$, Eq. (22) becomes linear, and its solution has the form

$$\Delta\bar{e}^{\mathrm{vp}} = \frac{q^{\mathrm{e}} - mp}{3G + \dfrac{mp}{\gamma\Delta t}}.$$

The pressure for time $t + \Delta t$, $p^{t+\Delta t}$, is calculated from the obvious formula

$$p^{t+\Delta t} = p^{t} + K\Delta\varepsilon_{ii}. \tag{23}$$

Calculations have been made for the following material data: Young's modulus $E = 1 \times 10^6$ Pa, Poisson's ratio $v = 0.3$, the angle of internal friction $\varphi = 25°$, viscosity parameters: $\gamma = 50\ \mathrm{s}^{-1}$, $N = 1$, mass density $\varrho = 1500\ \mathrm{kg/m}^3$. The angle of friction between the bulk material and silo walls and insert surface is set as $\varphi_w = 20°$.

The mesh of 8662 elements with 4481 nodes and 31,000 material points are introduced for one half of the cross-section of the silo in the case of the silo without inserts. For the silo with the insert these numbers are as follows: 9906 elements, 5140 nodes and 31,128 material points. The initial stress field is calculated by the use of FEM under the assumption that the gravity forces are applied quasi-statically.

The obtained flow patterns are shown in Figs. 4 and 5 for several time instants. The funnel flow is observed for the silo without an insert, while in the case of the insert, the mass flow is obtained for the upper part of the material. It can be seen from the figures that there is no difficulty with solving the self-contact problem for the granular material and the problem of its flow around the insert. It is noted that the problem of flow around insert is very difficult to solve when the Lagrangian formulation of the finite element method is used.

It is seen from the figures that application of inserts can change significantly the type of flow in the upper part of the silo—the mass flow is observed in the case of insert instead of the funnel flow in the case of the silo without an insert.

The analysis of the problem for the silo without inserts took 24.5 h of PC-computer equipped with 1.5 GHz processor. The time increment used in the calculations has been set as follows: $\Delta t = 2.5 \times 10^{-5}$ for $t \leqslant 0.8$ s and $\Delta t = 1.0 \times 10^{-5}$ for $0.8 < t \leqslant 1.25$ s. In the case of the silo with the insert, the calculation process took much more time: 182.9 h. The calculations were made for the following values of time increment: $\Delta t = 1.0 \times 10^{-5}$ for $t \leqslant 0.4$ s, $\Delta t = 5.0 \times 10^{-6}$ for $0.4 < t \leqslant 0.7$ s, and $\Delta t = 2.5 \times 10^{-6}$ for $0.7 < t \leqslant 2.0$ s.

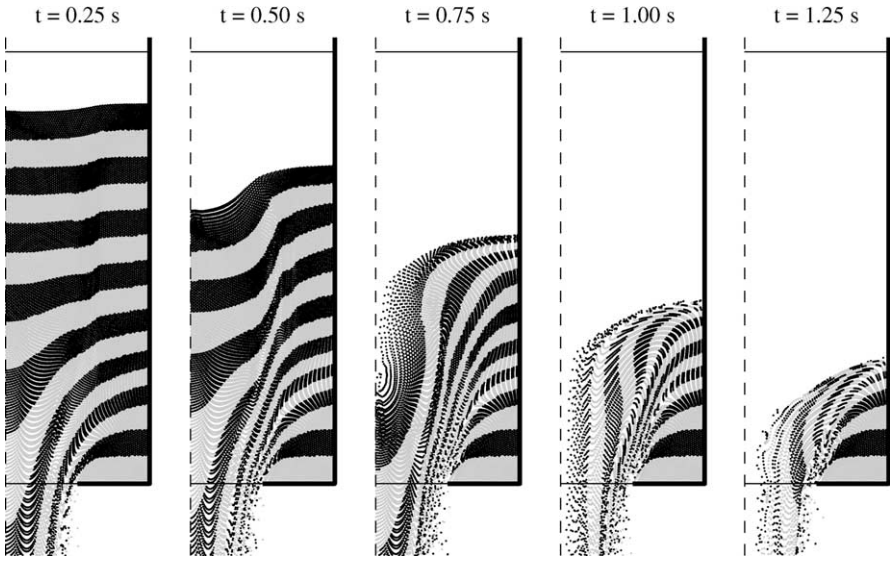

Fig. 4. Flow pattern—silo without insert.

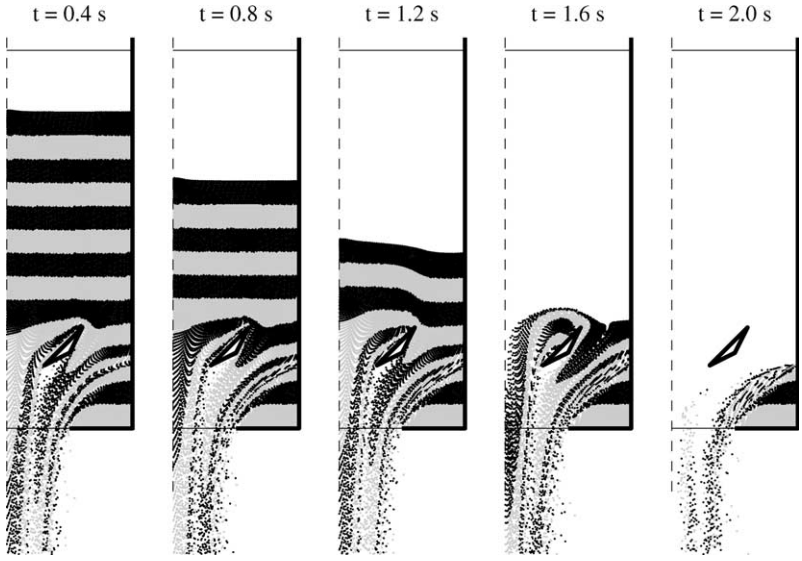

Fig. 5. Flow pattern—silo with insert.

5.1.2. Granular flow in silo—filling problem

It is assumed that a silo is filled by releasing portions of granular material of given mass and volume with given frequency. The initial position of these portions is fixed in space; the initial velocity and stress fields are equal to zero. The released material falls freely after start and then hits the bottom (wall) of the silo or the bulk material stored in it. In the analysis of the filling process, two constitutive concepts are utilized. The relation between the average normal stress (pressure, $p = -\sigma_{ii}/3$) and volume change is described as in

the Voigt model of a viscoelastic body, while for the relation between the deviatoric parts of the stress tensor and the tensor of deformation rate, the model of elastic–viscoplastic body is employed. For the non-cohesion material considered in the analysis, the relation between the pressure and the volume change, $\dot{\varepsilon}_{\mathrm{vol}}$, can be written in the following form:

$$p = p_0 \exp\left[\frac{1+e_0}{\kappa}(1-\exp\varepsilon_{\mathrm{vol}})\right] + (-\mu\dot{\varepsilon}_{\mathrm{vol}})^+, \tag{24}$$

where p_0 and e_0 denote pressure and void ratio for the state with respect to which the volume change is measured, κ is the elastic coefficient, μ the bulk viscosity ratio, the dot denotes the time partial derivative, and the brackets, $(\ )^+$, the positive part of an expression, $(x)^+ = \max(0,x)$. The elastic part of pressure p (the first component of the right hand side in Eq. (24)) follows from the linear relation between the void ratio and the pressure, well-known in soil mechanics (e.g. [52]):

$$e - e_0 = -\kappa \ln\frac{p}{p_0}.$$

The relation between the deviatoric parts of the rate-of-deformation and rate-of-stress tensors is defined by Eqs. (16)–(18). The only difference is that the shear modulus depends on the pressure,

$$G = \frac{3}{2}\frac{1-2v}{1+v}\frac{1+e_0}{\kappa}p\exp\varepsilon_{\mathrm{vol}}.$$

The procedure of time integration for the deviatoric part of stresses is the same as in the case of the material model considered in Section 5.1.1. The pressure is updated by explicit integration procedure applied to relation (24).

The plane strain problem is solved for a silo the cross-section of which is presented in Fig. 6, where the dimensions are given in centimetres. It is assumed that each released portion of the granular material occupies the cuboidal region $20\times10\times100$ cm^3 shown in Fig. 6 and its mass is 20 kg. The portions are released in 42 s with the step set as 0.2 s.

Calculations are made for the following material data: $\kappa = 0.02$, $v = 0.3$, $e_0 = 0.9$, $p_0 = 600$ Pa, $\varphi = 30°$, $\mu = 10^4$ Pa s, $\gamma = 10^4$ s^{-1}, $N = 1$, and mass density for the skeleton $\varrho_s = 2850$ kg/m^3. It is assumed that the angle of friction between the granular material and silo walls is set as $\varphi_w = 20°$.

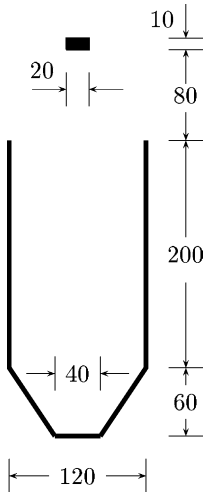

Fig. 6. Cross-section of silo—plane strain filling problem.

Because of the symmetry, only half of the cross-section of the silo is analysed. The total number of the material points defined has been set as 30,240 while the number of points in each released portion as 144 (12×12). The computational mesh has 1957 elements and 1056 nodes. The problem is solved with the time increment $\Delta t = 2 \times 10^{-5}$ s applied in the explicit procedure of time integration of the dynamic equations.

The deformation history is presented in Fig. 7 where each shown layer—except the last one—contains 576 material points released in four consecutive portions.

The tractions between the granular material and the silo walls and bottom are depicted in Fig. 8 for the same time instants as for which the deformation is shown in the previous figure. The normal and tangential

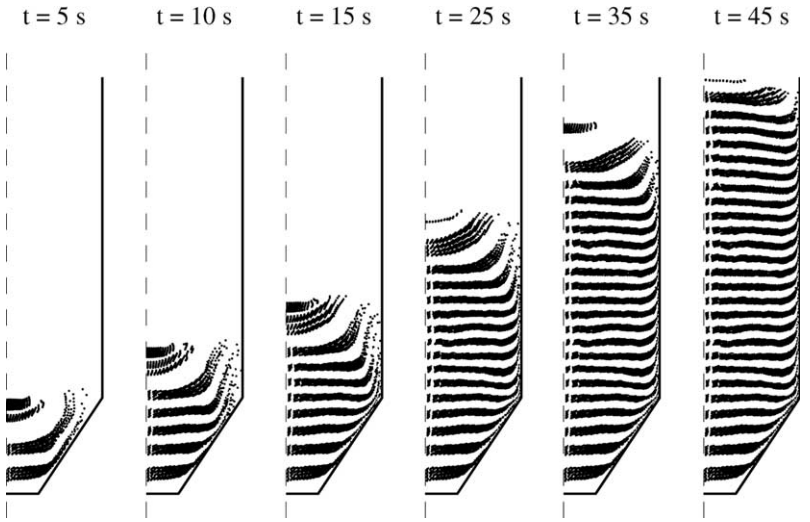

Fig. 7. Phases of filling process.

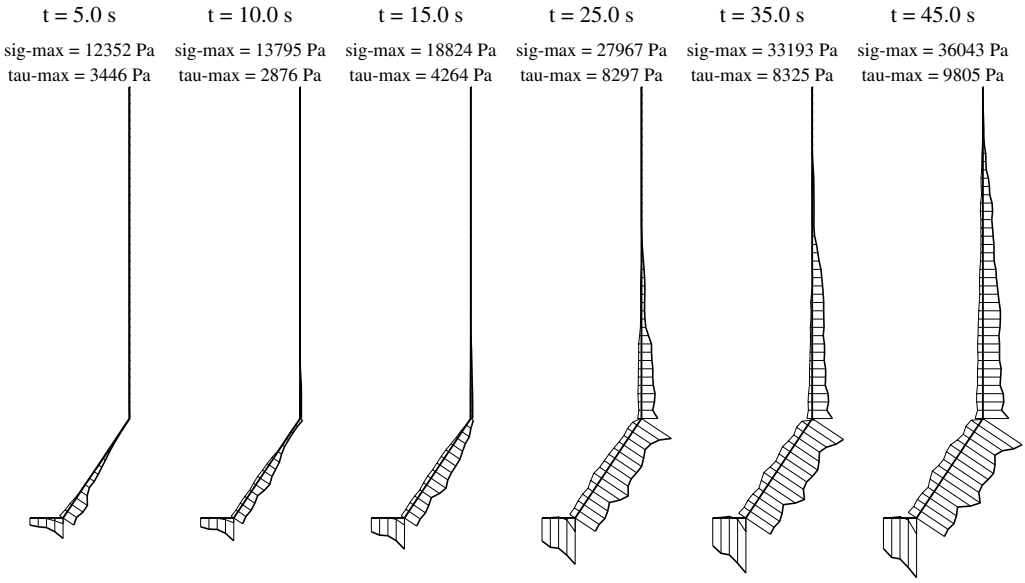

Fig. 8. Wall tractions in filling process.

tractions are represented by the thick and thin lines, respectively. The results obtained for the last shown phase of filling (45 s) are compared with those evaluated by the quasi-static finite element analysis and represented in Fig. 9. The largest differences are observed for the bottom of the silo.

The time of calculations exceeded 8 day and nights; a PC-computer with 1.5 GHz processor was used.

5.2. Retaining wall failure

The problem of failure of the retaining wall, shown in Fig. 10, is analysed. It is assumed that the concrete wall looses its ability to resists tension stresses in the bottom area filled in black colour in the figure. The walls are treated as elastic bodies for which the material parameters are as follows: $E = 2 \times 10^{10}$ Pa, $v = 0.17$, $\varrho = 2500$ kg/m^3. For the damaged part of the wall, the model of granular material described in Section 5.1.1 is applied with the data: $\varphi = 40°$, $\gamma = 100$ s^{-1}, $N = 1$. The mechanical behaviour of the stored material (region Ω_1) and the soil (region Ω_2) is described by the same material model. The material data is as follows:

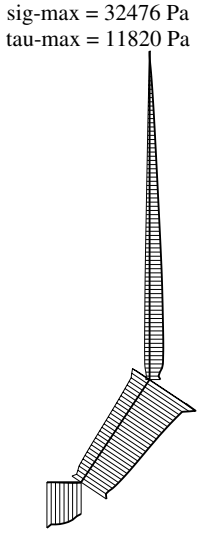

Fig. 9. Wall tractions—quasi-static solution.

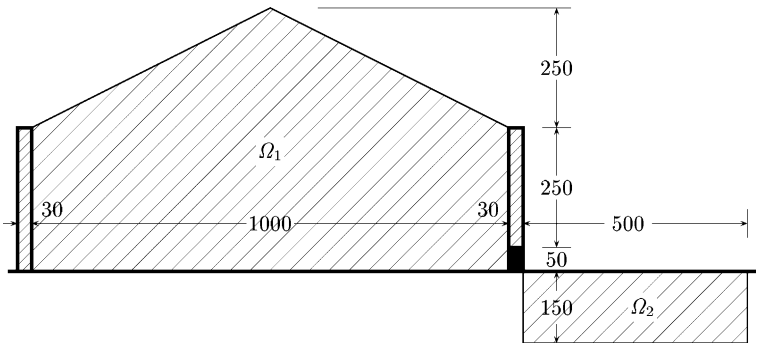

Fig. 10. Retaining wall failure—definition of the problem.

- the stored material: $E = 1 \times 10^6$ Pa, $\nu = 0.3$, $\varphi = 30°$, $\gamma = 100$ s^{-1}, $N = 1$, $\varrho = 1500$ kg/m^3,
- the soil: $E = 5 \times 10^6$ Pa, $\nu = 0.3$, $\varphi = 40°$, $\gamma = 100$ s^{-1}, $N = 1$, $\varrho = 1500$ kg/m^3.

Calculations have been made using 35,312 material points and the computational mesh with 5765 nodes and 11,204 triangular elements. The time increment has been set as follows: $\Delta t = 2.5 \times 10^{-5}$ s for $t \leqslant 1.3$ s, and $\Delta t = 1.0 \times 10^{-5}$ s for $t > 1.3$ s. Several stages of the collapse sequence are presented in Fig. 11. The points representing the retaining walls are plotted in black colour in the figure. The region occupied by the computational element mesh is indicated by dashed lines. The development of a shear band is observed in the figure. The shear band is initialised at the bottom of the collapsed wall and then spreads to the top of the stored material. One can notice that the problem of contact between the falling wall and the soil surrounding the storing structure is solved without difficulty. No trouble is observed in solving the problem of interaction between the stored granular material and the moving wall which behaves as almost rigid body.

The analysis of the process lasting 2 s took 40 h of a PC-computer equipped with 1.5 GHz processor.

5.3. Plastic forming

Two examples of metal plastic forming problems are considered: the extrusion and cutting problems. The elastic–perfectly plastic constitutive model with Huber–von Mises yield condition is applied in both the analyses.

5.3.1. Extrusion problem

The extrusion problem shown in Fig. 12 is considered; the plane strain problem is analysed. The dimensions presented in the figure are in millimetres. Neglecting thermal effects, the problem is solved with the following data: $E = 2 \times 10^5$ MPa, $\nu = 0.3$, plastic limit $\sigma_0 = 20$ MPa, $\varrho = 7800$ kg/m^3, $\mu = 0.1$, where μ denotes the coefficient of friction between the formed material and the tool surface. The total load was set as 800 kN/m.

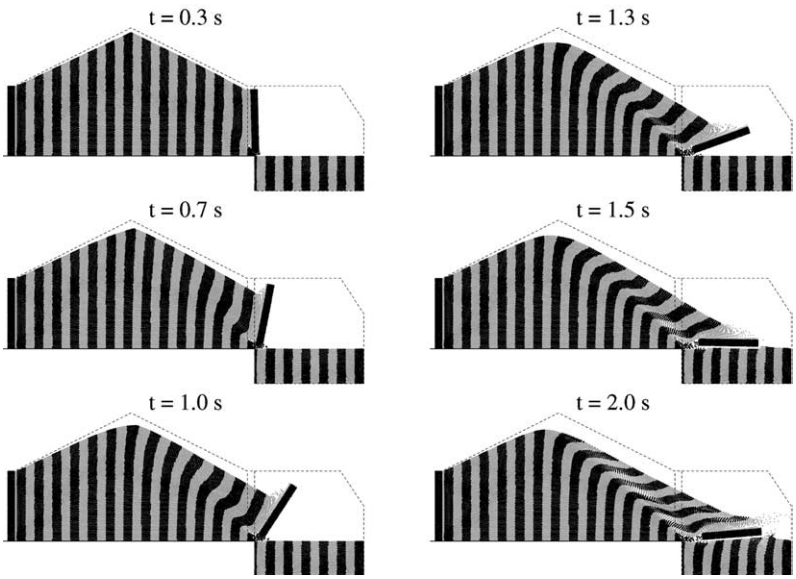

Fig. 11. Failure of retaining wall—stages of deformation.

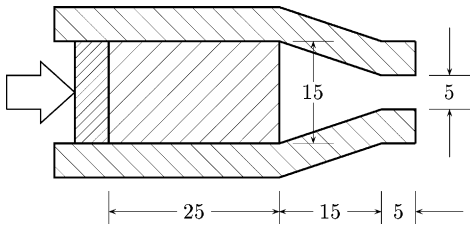

Fig. 12. Extrusion problem.

Owing to symmetry of the problem, only the upper half of the body is analysed, where 6750 material points is defined. The computational element mesh contains 4320 constant-strain elements and 2342 nodes; it is presented at the top of Fig. 13.

The results of the calculations are demonstrated in Fig. 13 where several phases of deformation are depicted. The smallest strains are observed in the neighborhood of the symmetry axis; the magnitude of the strains grows with the distance from the symmetry axis. The same observation follows from the results obtained by other methods, e.g. by the finite element method formulated in the Lagrangian format [53]. In the example, it is assumed that the force influences the formed material through a layer of a perfectly elastic material, and is applied to one material point located inside this layer. Using the material point method, it is also possible to apply forces at nodes of the computational mesh placed in the cross-section of the forming tool. Another possibility is to impose velocities at nodes of the computational mesh. The ALE features of the material point method makes various types of boundary conditions convenient to apply.

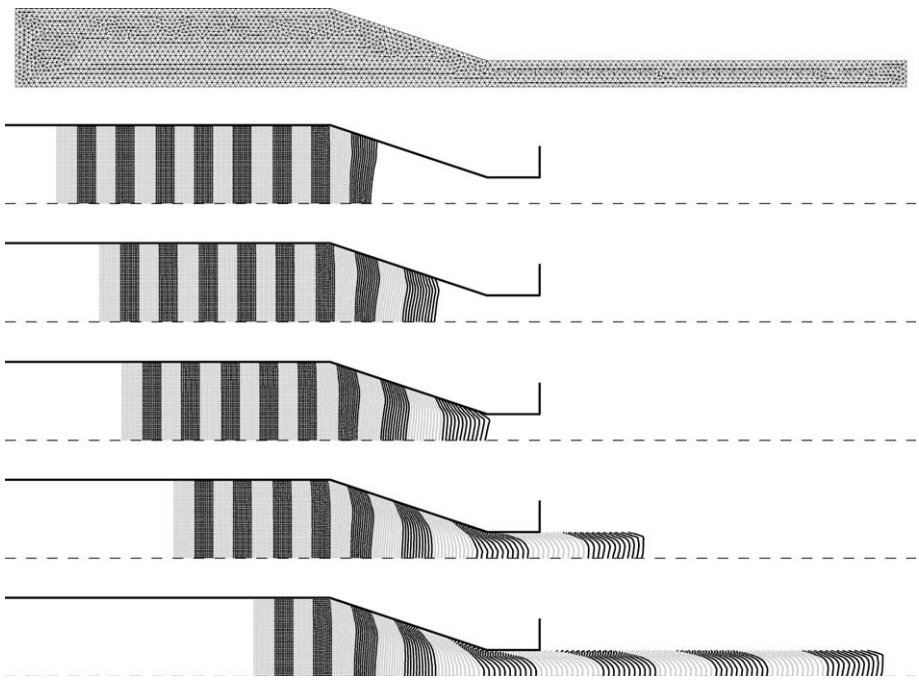

Fig. 13. Extrusion problem—computational mesh and deformation process.

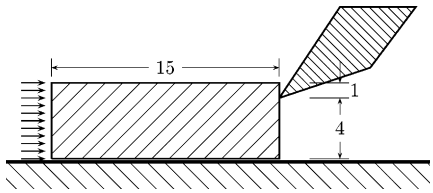

Fig. 14. Cutting problem.

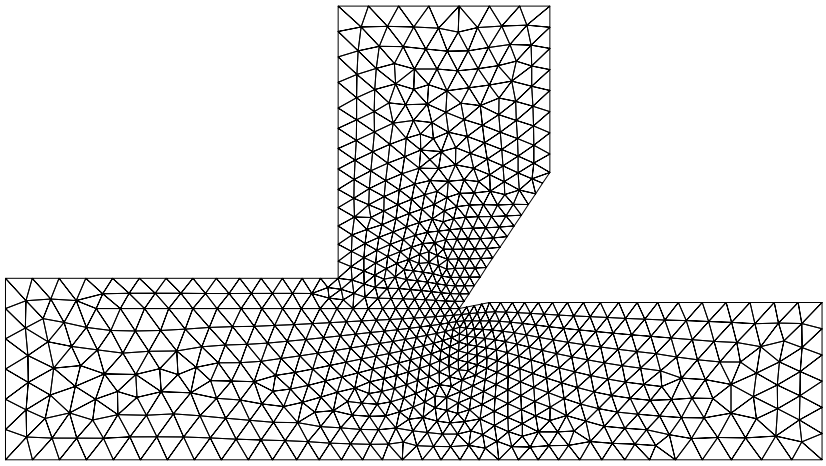

Fig. 15. Cutting problem—computational mesh.

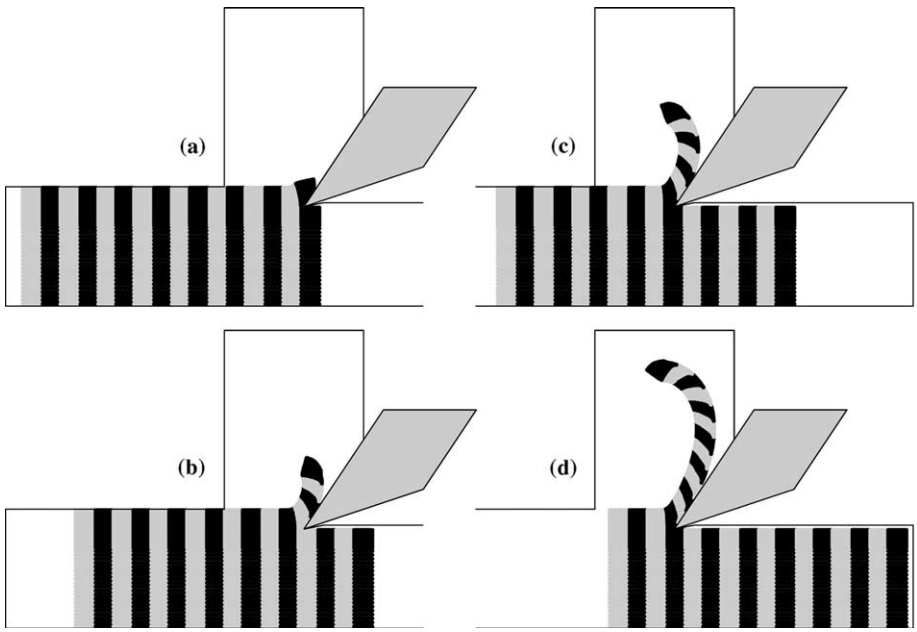

Fig. 16. Cutting problem—deformation process.

5.3.2. Cutting problem

The cutting problem is analysed in the example—the plane stress for the plate presented in Fig. 14 (dimensions shown in millimetres) is considered. As in the previous example, the analysis is done for the elastic–perfectly plastic material model with the Huber–von Mises yield condition. The material data is as follows: $E = 7.3 \times 10^4$ MPa, $\nu = 0.2$, $\sigma_0 = 50$ MPa, $\varrho = 2700$ kg/m^3. The coefficient of friction between the cut material and the cutting tool, μ, is equal to 0.1, and the load acting on the plate 100 kN/m. As in the previous example, the load is applied at material points. The load is applied at the material points grouped in one vertical row (the first one from the left).

The computational mesh, containing 1468 constant-strain triangular elements and 798 nodes, is applied in the calculations; 6000 material points are introduced. The mesh is depicted in Fig. 15.

The development of the cutting process is shown in Fig. 16. In the analysis, two nodes having the same coordinates are defined at the tip of the cutting tool. This enables to associate each of these nodes to one of the edges of the tool. Such a manner makes it possible to introduce different boundary conditions (or contact conditions) for these two nodes. Using this idea, a very smooth surface of the cut material is obtained as a result of the analysis. The numerical experiments show that the smoothness of the surface may be not perfect when only one node is introduced at the tip of the cutting tool.

6. Conclusions

The material point method—the variant of the finite element method formulated in an arbitrary Lagrangian–Eulerian (ALE) description of motion, is described in the paper and applied to such large strain engineering problems as granular flow and plastic forming problems. By comparison with earlier papers [36–39], the method has been enriched by adding the more accurate procedure evaluating the volume change of the analysed body which makes some problems, e.g. silo filling, possible to solve. The results shown in the paper prove that the method is a robust tool in the analysis of such complicated tasks as discharging and filling a silo, failure of retaining wall and modelling the forming problems for metals. Some problems like granular flow around a silo insert and the problem of self-contact of granular material can be solved in relatively easy way by the use of the material point method in contrast to the standard finite element method. The material point method looks very promising as a tool of analysis of other large strain problems like motion of avalanches and simulation of earth-moving processes. However, the method is time consuming. It seems that the use of parallel computation technique can reduce the time consumption of the method as calculations performed at the material points and elements level and the solution of system of algebraic equations, when the diagonalized mass matrix is utilized, can be parallelized easily.

Acknowledgement

This work was partly supported by the (Polish) State Committee for Scientific Research through the grant No. 7 T07A 006 17.

References

[1] W.E. Pracht, Calculating three-dimensional fluid flows at all speeds with an Eulerian–Lagrangian computing mesh, J. Comput. Phys. 17 (1975) 132–159.

[2] T.J.R. Hughes, W.K. Liu, T.K. Zimmerman, Lagrangian–Eulerian finite element formulation for incompressible viscous flows, Comput. Methods Appl. Mech. Engrg. 29 (1981) 329–349.

[3] T.B. Belytschko, D.P. Flanagan, J.M. Kennedy,, Finite element methods with user controlled mesh for fluid structure interaction, Comput. Methods Appl. Mech. Engrg. 33 (1982) 669–688.
[4] J. Donea, Arbitrary Lagrangian–Eulerian finite element methods, in: T.B. Belytschko, T.J.R. Hughes (Eds.), Computational Methods for Transient Analysis, Elsevier Science Publishers, Amsterdam, 1983, pp. 473–516.
[5] J. van der Lugt, J. Huetink, Thermo-mechanically coupled finite element analysis in metal forming processes, Comput. Methods Appl. Mech. Engrg. 54 (1986) 145–160.
[6] P.J.G. Schreurs, F.E. Veldpaus, W.A.M. Brekelmans, Simulation of forming processes, using the arbitrary Eulerian–Lagrangian formulation, Comput. Methods Appl. Mech. Engrg. 58 (1986) 19–36.
[7] W.K. Liu, T. Belytschko, H. Chang, An arbitrary Lagrangian–Eulerian finite element method for path-dependent materials, Comput. Methods Appl. Mech. Engrg. 58 (1986) 227–246.
[8] W.K. Liu, H. Chang, T. Belytschko, Arbitrary Lagrangian–Eulerian and Eulerian Petrov–Galerkin finite elements for nonlinear continua, Comput. Methods Appl. Mech. Engrg. 68 (1988) 259–310.
[9] W.K. Liu, J.S. Chen, T. Belytschko, Y.F. Zhang, Adaptive ALE finite elements with particular reference to external work rate on frictional interface, Comput. Methods Appl. Mech. Engrg. 93 (1988) 189–216.
[10] A. Huerta, W.K. Liu, Viscous flow with large free surface motion, Comput. Methods Appl. Mech. Engrg. 69 (1988) 277–324.
[11] D.J. Benson, An efficient accurate simple ALE method for nonlinear finite element programs, Comput. Methods Appl. Mech. Engrg. 72 (1996) 205–350.
[12] T. Belytschko, W.K. Liu, B. Moran, Nonlinear Finite Elements for Continua and Structures, Wiley & Sons, Chichester, 2000.
[13] T.J. Liszka, J. Orkisz, The finite difference method at arbitrary irregular grids and its applications in applied mechanics, Comput. Struct. 11 (1980) 83–95.
[14] J. Orkisz, Meshless finite difference method. I. Basic approach, in: S.R. Idelsohn, E. Oñate, E.N. Dvorkin (Eds.), Proceedings of IV World Congress on Computational Mechanics, Buenos Aires, June 29–July 2 1998.
[15] J. Orkisz, Meshless finite difference method. II. Adaptive approach, in: S.R. Idelsohn, E. Oñate, E.N. Dvorkin (Eds.), Proceedings of IV World Congress on Computational Mechanics, Buenos Aires, June 29–July 2 1998.
[16] B. Nayroles, G. Touzot, P. Villon, Generalizing the finite element method: Diffuse approximation and diffuse elements, Comput. Mech. 10 (1992) 307–318.
[17] T. Belytschko, Y.Y. Lu, L. Gu, Element-free Galerkin methods, Int. J. Numer. Methods Engrg. 37 (1994) 229–256.
[18] K. Jach, J. Leliwa–Kopystyński, M. Mroczkowski, R. Świerczyński, P. Wolański, Free particle modelling of hypervelocity asteroid collisions with the earth, Planet. Space Sci. 42 (1994) 1123–1137.
[19] E. Oñate, S. Idelsohn, O.C. Zienkiewicz, R.L. Taylor, C. Sacco, A stabilized finite point method for analysis of fluid mechanics problems, Comput. Methods Appl. Mech. Engrg. 139 (1996) 315–346.
[20] S.N. Atluri, T. Zhu, A new meshless local Petrov–Galerkin (MLPG) approach in computational mechanics, Comput. Mech. 22 (1998) 117–127.
[21] T. Zhu, J. Zhang, S.N. Atluri, A meshless local boundary integral equation (LBIE) method for solving nonlinear problems, Comput. Mech. 22 (1998) 174–186.
[22] L.B. Lucy, A numerical approach to the testing of the fission hypothesis, Astron. J. 8 (1977) 1013–1024.
[23] J.J. Monaghan, An introduction to SPH, Comput. Phys. Commun. 48 (1988) 89–96.
[24] L.D. Libersky, A.G. Petschek, A.G. Carney, T.C. Hipp, F.A. Allahdadi, High strain Lagrangian hydrodynamics—a three-dimensional SPH code for dynamic material response, J. Comput. Phys. 109 (1993) 67–75.
[25] G.R. Johnson, R.A. Stryk, S.R. Beissel, SPH for high velocity impact computations, Comput. Methods Appl. Mech. Engrg. 139 (1996) 347–373.
[26] P.W. Randles, L.D. Libersky, Smoothed particle hydrodynamics: Some recent improvements and applications, Comput. Methods Appl. Mech. Engrg. 139 (1996) 375–408.
[27] W.K. Liu, S. Jun, S. Li, J. Adee, T. Belytschko,, Reproducing kernel particle methods for structural dynamics, Int. J. Numer. Methods Engrg. 38 (1995) 1655–1679.
[28] J.S. Chen, C. Pan, C.T. Wu, W.K. Liu, Reproducing kernel particle methods for large deformation analysis of non-linear structures, Comput. Methods Appl. Mech. Engrg. 139 (1996) 195–227.
[29] J.M. Melenk, I. Babuška, The partition of unity finite element method: Basic theory and applications, Comput. Methods Appl. Mech. Engrg. 139 (1996) 289–314.
[30] C.A. Duarte, J.T. Oden, An *h–p* adaptive method using clouds, Comput. Methods Appl. Mech. Engrg. 139 (1996) 237–262.
[31] T.J. Liszka, C.A.M. Duarte, W.W. Tworzydło, *hp*-Meshless cloud method, Comput. Methods Appl. Mech. Engrg. 139 (1996) 263–288.
[32] O.C. Zienkiewicz, R.L. Taylor, The Finite Element Method, vol. 1, fifth ed., Butterworth–Heinemann, Oxford, 2000.
[33] G.R. Liu, Mesh Free Methods: Moving Beyond the Finite Element Method, CRC Press, 2001.
[34] F.H. Harlow, The particle-in-cell computing method for fluid dynamics, in: B. Adler, S. Fernbach, M. Rotenberg (Eds.), Methods for Computational Physics, vol. 3, Academic Press, New York, 1964, pp. 319–343.

[35] D. Burgess, D. Sulsky, J.U. Brackbill, Mass matrix formulation of the FLIP particle-in-cell method, J. Comput. Phys. 103 (1992) 1–15.
[36] D. Sulsky, Z. Chen, H.L. Schreyer, A particle method for history-dependent materials, Comput. Methods Appl. Mech. Engrg. 118 (1994) 179–196.
[37] D. Sulsky, S.-J. Zhou, H.L. Schreyer, Application of a particle-in-cell method to solid mechanics, Comput. Phys. Commun. 87 (1995) 236–252.
[38] D. Sulsky, H.L. Schreyer, Axisymmetric form of the material point method with applications to upsetting and Taylor impact problems, Comput. Methods Appl. Mech. Engrg. 139 (1996) 409–429.
[39] Z. Więckowski, S.K. Youn, J.H. Yeon, A particle-in-cell solution to the silo discharging problem, Int. J. Numer. Methods Engrg. 45 (1999) 1203–1225.
[40] T.J.R. Hughes, The Finite Element Method. Linear Static and Dynamic Finite Element Analysis, Prentice Hall, Englewood Cliffs, NJ, 1987.
[41] O.C. Zienkiewicz, R.L. Taylor, The Finite Element Method, vol. 2, fifth ed., Butterworth–Heinemann, Oxford, 2000.
[42] U. Häussler, J. Eibl, Numerical investigation on discharging silos, J. Engrg. Mech. ASCE 110 (1984) 957–971.
[43] J. Eibl, G. Rombach, Numerical investigation on discharging silos, in: G. Swoboda (Ed.), Proceedings of 6th International Conference on Numerical Methods in Geomechanics, Balkema, 1988, pp. 317–320.
[44] K. Runesson, L. Nilsson, Finite element modelling of the gravitational flow of a granular material, Int. J. Bulk Solids Handling 6 (1986) 877–884.
[45] S.A. Elaskar, L.A. Godoy, D.D. Gray, J.M. Stiles, A viscoplastic approach to model the flow of granular solids, Int. J. Solid Struct. 37 (2000) 2185–2214.
[46] Z. Więckowski, M. Klisiński, Finite deformation analysis of motion of granular materials in a silo, Arch. Mech. 47 (1995) 617–633.
[47] P.A. Langston, U. Tüzün, D.M. Heyes, Discrete element simulation of granular flow in 2D and 3D hoppers: Dependence of discharge rate and stress on particle interactions, Chem. Eng. Sci. 50 (1995) 967–987.
[48] D.R.J. Owen, Y.T. Feng, P.A. Klerck, J. Yu, A.J.L. Crook, Computational strategies for multi-fracturing solids and particulate media, in: Proceedings of 2nd European Conference on Computational Mechanics, ECCOMAS, IACM, Cracow, 2001, CD-ROM.
[49] H.-B. Mühlhaus, H. Sakaguchi, L. Moresi, M. Fahey, Discrete and continuum modelling of granular materials, in: P.A. Vermeer, S. Diebels, W. Ehlers, H.J. Herrmann, S. Luding, E. Ramm (Eds.), Continuous and Discontinuous Modelling of Cohesive–Frictional Materials, Springer, Berlin, 2001, pp. 185–204.
[50] L. Oger, S.B. Savage, M. Sayed, Granular flow using particle-in-cell approach, in: Proceedings of 4th Euromech Conference, Metz, 2000, Vol. 1, p. 126.
[51] P. Perzyna, Fundamental problems in visco-plasticity, Adv. Appl. Mech. 9 (1966) 243–377.
[52] A. Schofield, C.P. Wroth, Critical State Soil Mechanics, McGraw-Hill, New York, 1968.
[53] R. Hambli, D. Badie-Levet, Damage and fracture simulation during the extrusion processes, Comput. Methods Appl. Mech. Engrg. 186 (2000) 109–120.